Comparison of computed tomograph and optical scanners for elements manufactured by Wire Arc Additive Manufacturing

xxxx

Abstract. Additive techniques become more and more common in manufacturing processes. Among metallic materials an interesting technique for depositing metallic layers is the use of Wire Arc Additive Manufacturing process, where 3D metallic structures are created using welding technologies, i.e. Gas Metal Arc Welding. In the paper an analysis of measurement devices for surfaces after that kind of manufacturing was presented. A computer tomograph as well as two types of scanners were used, respectively with a high and low resolution. For dimensional measurements the results showed that a CT is a good option, enabling to properly represent the real work piece. The results obtained with a high resolution scanner were usually pretty close, except for few cases. On the other hand, a low resolution scanner due to a large distance between points was not able to show good dimensions. Pores in structures were also inspected. The biggest problems with pores occurred where path of a robotic arm was the most complicated.

Keywords: Wire Arc Additive Manufacturing, Scanner, Computer Tomograph.

1 Introduction

Additive techniques are gaining popularity in manufacturing processes [1, 2, 3]. Both techniques using plastics [4] and metal materials [5] are used. The multitude of techniques associated with manufacturing include methods of Selective Laser Sintering (SLS), Digital Light Processing (DLP), Fused Filament Fabrication (FFF), Direct Metal Laser Sintering (DMLS), VAT Photopolymerization (VPP), Material Jetting Additive (MJT), Binder Jetting (BJT), Powder Bed Fusion (PBF), Material Extrusion (MEX) or Directed Energy Deposition (DED). Among metallic materials, powder sintering [6], laser [7] or electron beam forming [8] and deposition [9] are the dominant methods. In the latter group of methods, an interesting technique for depositing metallic layers is the use of Wire Arc Additive Manufacturing (WAAM) process [10], where 3D metallic structures are created using welding technologies [11], i.e. Gas Metal Arc Welding (GMAW) [12]. Generally speaking, Additive Layer Manufacturing, including Wire and Arc Additive Layer Manufacture (WAALM) became an interesting and important technology which is more and more often used in industrial processes. It can be used to manufacture work pieces out of many different materials, answering a demand for sustainable, low cost and environmentally friendly manufacturing processes with very high geometric flexibility. Deposition of materials with Wire and Arc Additive Layer

Manufacture comprise of e.g. steel [13], Ni alloys [14], and Ti alloys [15]. The process can be run with various welding parameters [16] and - as a usual modern welding operation - is usually performed with a robot [17].

2 Measurement techniques in additive manufacturing

Additive techniques do not always allow the use of classical measurement methods [18]. Some features obtained as a result of them also require a special mathematical approach [19]. Measurements of structures obtained by these techniques on a macro scale more justify the use of measurement methods based on electromagnetic radiation than contact techniques. Therefore, in this paper, optical scanners of different resolution and a computer tomograph were used for measurements.

Coordinate measuring machines in macro scale have gained popularity over a number of years and have become indispensable in various industries. But coordinate measuring technology has gone much further in recent years. The variety of measurement tasks and complex shapes of workpieces have led to the development of optical measuring tools that allow to solve problems that are difficult to realize with contact methods. These include 3D scanners. Their great advantage is the speed of acquiring an enormous amount of information on the product being measured and the clarity of the presentation of the results. They are based on the principle of measuring the light reflected or scattered from the surface of the measured object and triangulation. We divide them basically into structural light scanners and laser ones. Structured light scanners [20, 21] are based on the projection of structured light, i.e. their projectors project patterns of e.g. Grey codes, phase shifted bars or other code forms (free shapes, circles, etc.) onto the measured surface. They are usually mounted on tripods. They are quite common in many different applications, including not only mechanical engineering [22], but also biomedicine [23], surface defects [24], concrete [25] or casting cores [26]. In many applications, structured light scanners are being increasingly replaced by newer solutions, namely laser scanners [27, 28]. Initially, solutions based on laser action were just laser scanning heads [29, 30] or laser triangulation heads, that were placed, for example, on CMMs or measuring arms. Currently, they function as standalone laser scanners [31] operating in manual or automatic mode and are one of the most common and effective data acquisition methods in a wide variety of applications [32], including also analysis of wire arc hybrid manufacturing process [33]. The working principle of laser scanning heads is based on emitting a point, a line or a set of laser lines on the surface of the scanned object. These elements are observed by the CCD camera giving coordinates of measurement points. They avoid problems associated with vibration and scanning from the so-called "free hand" and are less sensitive to light reflections. A schematic picture of example laser scanners is shown in figure 1 [34].

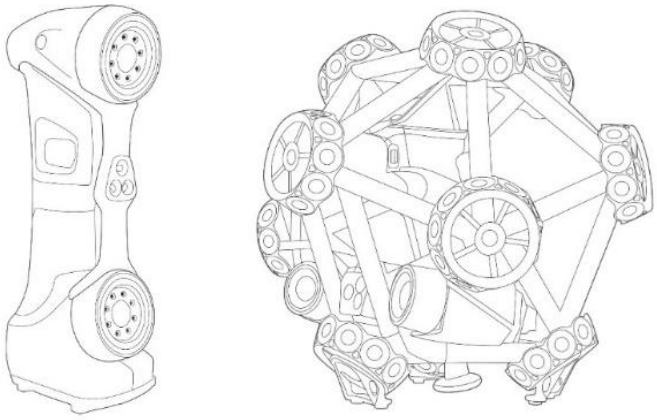

Fig. 1. Schematic image of laser scanners.

Electromagnetic radiation can be used in metrology not only in the visible range. Computed tomography [35], which is based on X-rays, is increasingly used not only to analyze defects but also geometrical features. Technical tomographs, allow imaging with a resolution even below a micrometer [36]. The classical system consists of a measured object placed on a rotating table and the lamp and detector that are stationary or perform linear motion. The radiation beam is attenuated as it passes through the object, and this process depends on the thickness of the absorbing medium and the absorption coefficient. During the measurement, a number (usually hundreds or thousands) of 2D X-ray images are taken for different angular positions of the lamp-detector system relative to the measured object [37]. As a result of reconstruction from 2D shots, a spatial image is obtained. Technical tomographs are used for the analysis of very different elements, including objects made of plastic [38], foam [39], and metal, also those made with additive techniques [40]. In this case, the analytical results are often better than those obtained by metallography [41]. Also the accuracy parameters [42] and the results of comparisons with other measurement methods used in coordinate technology [43] make this application future of computed tomography look very positive.

3 Materials and measures

A robotic additive manufacturing system using GMAW was used in this study. The test samples were made out of S235 JR steel using AWS ER70S-6 wire material and 15% CO2 and 85% argon gas composition. The torch provided a flux of gas during the welding process and also during a brief period, before arc establishment and after the end of it. It ensures that the material is protected from oxidation every time. The samples were made with 40A intensity, 5V voltage, 310 mm/min feed rate and 1,7 m/min wire speed. There were three different shapes of samples, prepared to show various opportunities of GMAW. Their nominal forms are presented on figure 2.

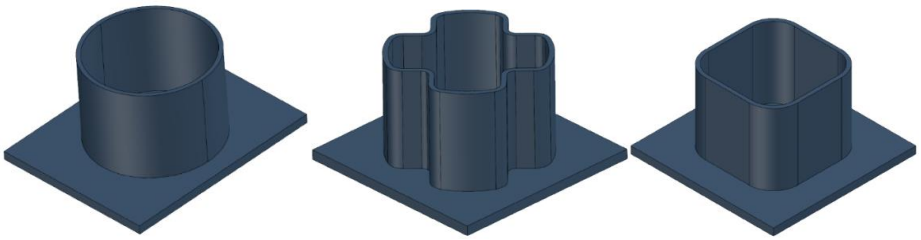

Fig. 2. Nominal shapes of samples.

For each type of shape (cylinder, cross and rectangle) three specimens were manufactured. The examples are presented on figure 3.

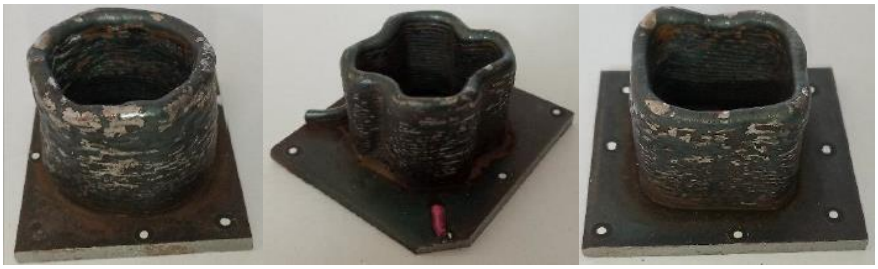

Fig. 3. Images of samples with cylindrical, rectangle and cross shape.

Cylinders were prepared to a nominal inner diameter of 22 mm and an outer diameter of 33 mm, assuming maximum inscribed element for inner diameters and minimum circumscribed element for outer diameter. Crosses had an inner diameter of 18 mm and an outer diameter of 33 mm, evaluated the same way. For rectangles, X and Y directions were determined, for which the nominal dimensions were: outer dimension X - 28 mm, inner dimension X - 21 mm, outer dimension Y - 26 mm, inner dimension Y - 19 mm. To investigate possibilities of digitization three different measurement devices were used; two optical structural light scanners and a computer tomograph. The scanners were selected with different resolutions, to verify an influence of resolution on image and data quality. The low resolution scanner (LRS) had a resolution of 0,5 mm, while the high resolution scanner (HRS) enabled to collect data with 0,115 mm measuring point distance. For computed tomography (CT) measurements, a 320W directional open-type lamp with a 200 μm pixel size detector was used. Measurements were performed at 230 kV and 200 μA current, and 1000 images were taken per rotation. Data were collected with a voxel size of 50,375 μm.

4 Results and discussion

The first study examined the differences in shape representation and dimensions for each type of work piece. All the samples were aligned to their nominal shapes. The alignments were shown on figure 4.

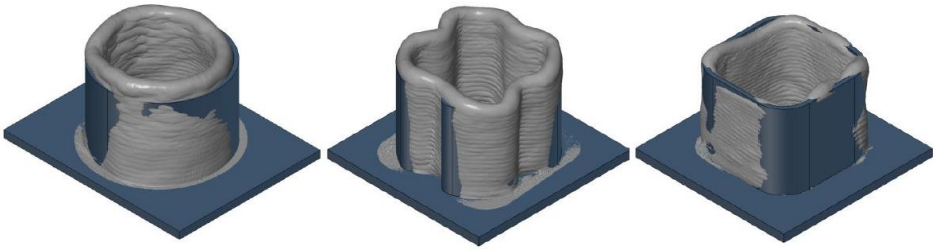

Fig. 4. Examples of alignment for different geometries: cylinder, cross and rectangle.

The results obtained for the cylinders are presented in Tables 1 and 2.

Table 1. Comparison of inner diameter (in mm) for cylinders (nominal 22 mm).

	Computed Tomograph CT	High Res Scanner HRS	Low Res Scanner LRS
Cylinder 1	21,607	21,592	21,743
Cylinder 2	23,823	23,855	23,772
Cylinder 3	22,521	22,538	23,089

Table 2. Comparison of outer diameter (in mm) for cylinders (nominal 33 mm).

	Computed Tomograph CT	High Res Scanner HRS	Low Res Scanner LRS
Cylinder 1	33,089	33,167	32,808
Cylinder 2	32,805	32,831	33,642
Cylinder 3	33,875	33,830	33,296

The images of work pieces are presented on figure 5.

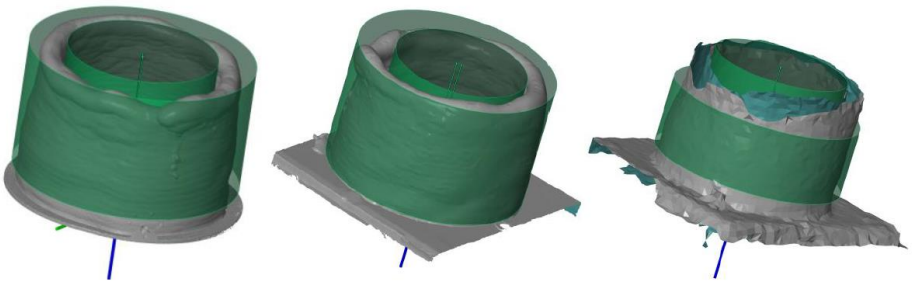

Fig. 5. Examples of diameter measurement for cylinders, from left to right: computed tomograph, high resolution scanner, low resolution scanner.

As can be seen from the presented data, the differences in dimensions between HRS and CT except for one case do not exceed 30 μm. However, for LRS the deviations are much larger and exceed even 0.5 mm. The images of cylinders retrieved by measuring devices show similar shapes for CT and HRS, while LRS had problems with identification of upper regions.

The same procedure was applied to cross shaped elements. The obtained results are presented in Tables 3 and 4.

Table 3. Comparison of inner diameter (in mm) for crosses (nominal 18 mm).

	Computed Tomograph CT	High Res Scanner HRS	Low Res Scanner LRS
Cross 1	17,706	17,676	18,396
Cross 2	18,268	18,296	18,793
Cross 3	18,272	18,255	18,946

Table 4. Comparison of outer diameter (in mm) for crosses (nominal 33 mm).

	Computed Tomograph CT	High Res Scanner HRS	Low Res Scanner LRS
Cross 1	33,088	33,120	32,506
Cross 2	33,184	33,191	32,478
Cross 3	33,061	33,087S	32,078

The images of work pieces are presented on figure 6.

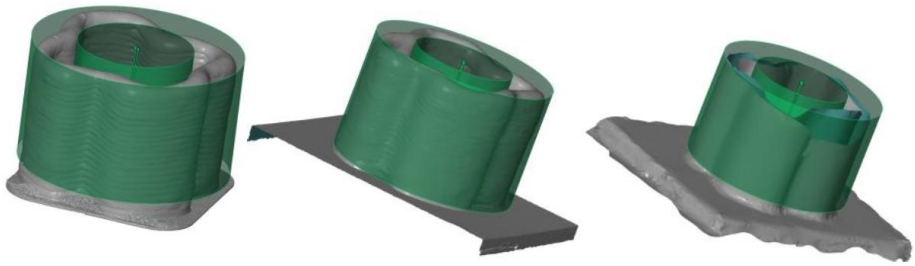

Fig. 6. Examples of diameter measurement for crosses, from left to right: computed tomograph, high resolution scanner, low resolution scanner.

For these surfaces, the dimensional difference between HRS and CT is similar to that for cylinders and ranges from 7 to 32 μm. For LRS the deviations are again much larger and reach up to 1 mm. The images of surfaces obtained by measuring devices similarly as before show similar shapes for CT and HRS, also here LRS had problems with identification of upper fragments, although smaller than in case of cylindrical surfaces. This is due to the fact that the surfaces are wider in places where the robot changes direction of its movement, making the LRS measurement task easier.

A measurement procedure for rectangles included measurements of internal and external dimensions in two mutually perpendicular directions, perpendicular also to the sides of the figures. The obtained results are presented in Tables 5 and 6.

Table 5. Comparison of inner dimensions (in mm) for crosses (nominal X=21 mm; Y=19 mm).

	Computed Tomograph CT		High Res Scanner HRS		Low Res Scanner LRS	
	X	Y	X	Y	X	Y
Rectangle 1	21,099	18,840	21,401	18,113	22,171	20,004
Rectangle 2	20,932	18,784	20,698	19,188	21,519	20,077
Rectangle 3	20,858	18,483	21,105	19,216	21,603	20,020

Table 6. Comparison of outer dimensions (in mm) for crosses (nominal X=28 mm; Y=26 mm).

	Computed Tomograph CT		High Res Scanner HRS		Low Res Scanner LRS	
	X	Y	X	X	Y	X
Rectangle 1	27,569	26,116	27,529	26,285	26,841	25,557
Rectangle 2	28,111	26,773	27,672	26,532	26,958	25,345
Rectangle 3	28,058	26,444	27,538	26,173	26,925	25,409

The images of work pieces are presented on figure 7.

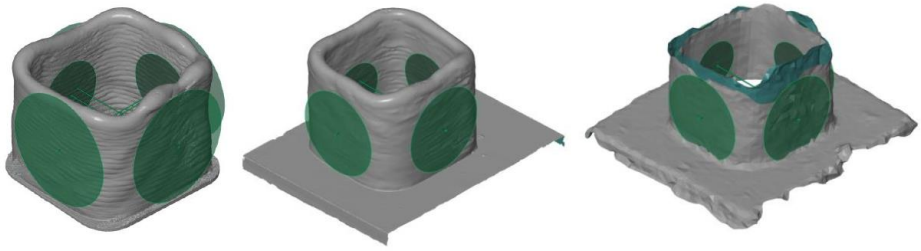

Fig. 7. Examples of diameter measurement for rectangles, from left to right: computed tomograph, high resolution scanner, low resolution scanner.

For these surfaces, the inner and outer dimension were analyzed in two directions. For the inner dimension, the differences between HRS and CT were large, up to 0.7 mm in the Y axis. The LRS on the other hand differed from the CT even more, up to about 1.5 mm. These differences show that for both scanners, the correct representation of the inner surface of a relatively small hole was a difficulty, which is natural when triangulation of this type of surface is concerned. The differences in the outer surfaces measured by CT and HRS were smaller and in most cases did not exceed 0.2 mm, which however is still significantly larger than the corresponding differences for the cylindrical and cross shaped surfaces. The reason for this phenomenon can be seen in the surface images, because HRS much less reliably reproduced the irregularities of the outer surface, i.e., phenomena occurring at the meso and micro scale. LRS also in this case showed large differences from the dimensions obtained with CT, with values reaching almost 1.5 mm. Also on these objects the LRS had great problems in identifying the top fragments.

From the images, it can be seen, that the thickness is growing when the layers are superposing. Due to that, there is the thinnest part in every sample located close to the plate. The values of thickness were calculated for each sample, as maximum, minimum and average. For cylinders, the results are presented in table 7.

Table 7. Comparison of thickness values for a cylinder.

	Computed Tomograph CT	High Res Scanner HRS	Low Res Scanner LRS
Maximum	3,461	3,250	3,413
Minimum	1,317	1,835	2,061
Average	2,663	2,715	2,625

The images of work pieces are presented on figure 8.

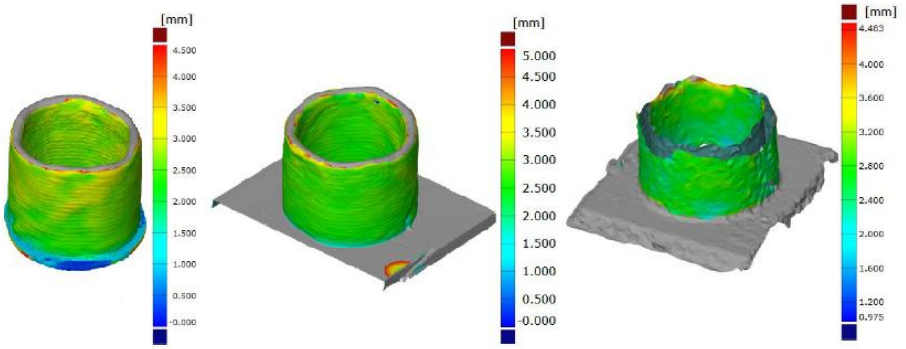

Fig. 8. Examples of thickness measurement for the cylinder, from left to right: computed tomograph, high resolution scanner, low resolution scanner.

The obtained differences show relatively good convergence for all three devices for maximum and average thickness. Bigger differences can be seen in the minimum thickness, and the larger values for HRS and LRS than for CT show that the scanners cannot quite good represent some of the valleys on the surfaces, tending to filter them out (LRS obviously filters out more). The surface images similarly show that the LRS resolution was not sufficient to represent the wall thickness of the cylinder.

The same procedure was also applied to cross shaped elements. The obtained results are presented in Table 8.

Table 8. Comparison of thickness values for a cross shaped element.

	Computed Tomograph CT	High Res Scanner HRS	Low Res Scanner LRS
Maximum	3,592	3,553	3,003
Minimum	1,149	1,790	2,036
Average	2,881	2,895	2,490

The images of the cross shaped work piece are presented on figure 9.

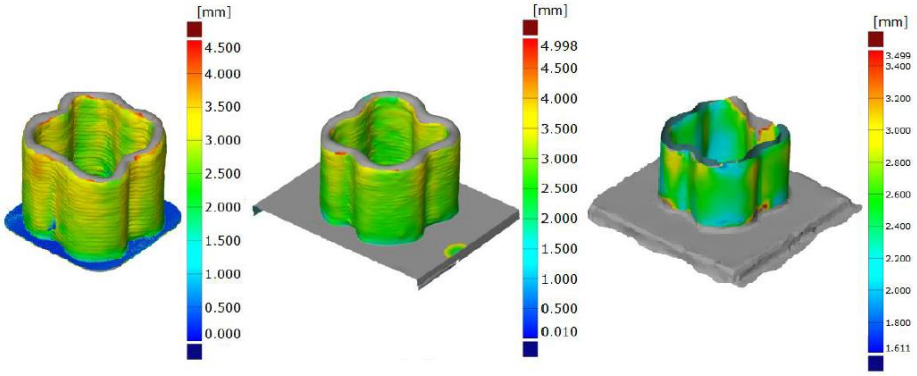

Fig. 9. Examples of thickness measurement for the cross shaped element, from left to right: computed tomograph, high resolution scanner, low resolution scanner.

The differences obtained show a relatively good convergence for CT and HRS for maximum and average thickness, in this case LRS showed smaller values, what - as previously - is related to the difficulty of mapping a complex surface. Big differences can again be seen in the minimum thickness, and here too larger values were obtained for HRS and LRS than for CT. On cross shaped surfaces there are more valleys and pitches, making it even more difficult for the scanners to image correctly, causing a filtering effect (again the LRS filters more). In the surface images, also in this case, the problems of LRS with the resolution and - consequently - the representation of the wall thickness of the element are clearly noticeable.

An analogous procedure was used to measure the wall thickness of elements made in rectangular shape. The results obtained for this element are presented in Table 9.

Table 9. Comparison of thickness values for a rectangle.

	Computed Tomograph CT	High Res Scanner HRS	Low Res Scanner LRS
Maximum	3,685	3,345	3,097
Minimum	0,865	1,810	1,815
Average	2,813	2,737	2,329

The images of the cross shaped work piece are presented on figure 10.

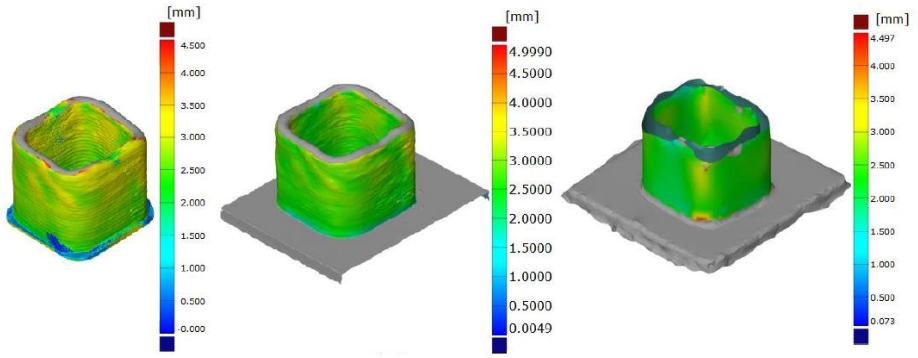

Fig. 10. Examples of thickness measurement for the rectangle, from left to right: computed tomograph, high resolution scanner, low resolution scanner.

The differences obtained show good convergence for CT and HRS for the average thickness, a little worse for the maximum thickness. The image obtained from HRS shows a very smoothed outer surface compared to reality. The LRS again showed smaller values related to mapping difficulty, although the differences are less significant than for the previous surfaces. The big differences are again in the minimum thickness, with larger values for the scanners. Interestingly, both showed very similar values, which may indicate similar problems in identifying the interior of the object. As in all cases there are also LRS problems with mapping the wall thickness of the part.

A crucial feature that is related with an additive process of production, is the porosity. For that reason, an analysis of the entire sample using a CT was performed. What is clear, this analysis is not possible with optical scanners. Table 10 shows the volume of voids that the was found during the scanning process. In the table, vacuum volume (mm3) means the summation of voids volume in the whole specimen, vacuum volume (%) represents the percentage of the summation of voids volume in relation to the total sample volume, and maximum pore diameter shows maximum diameter of the biggest internal void.

Table 10. Porosity of samples.

	Vacuum Volume (mm^3)	Vacuum volume (%)	Maximum pore diameter (mm)
Cylinder 1	No voids	No voids	No voids
Cylinder 2	No voids	No voids	No voids
Cylinder 3	No voids	No voids	No voids
Cross 1	0,001	0,000	0,194
Cross 2	5,176	0,093	2,120
Cross 3	No voids	No voids	No voids
Rectangle 1	No voids	No voids	No voids
Rectangle 2	0,018	0,001	0,460
Rectangle 3	No voids	No voids	No voids

The X-ray images of the samples with pores were presented on figure 11.

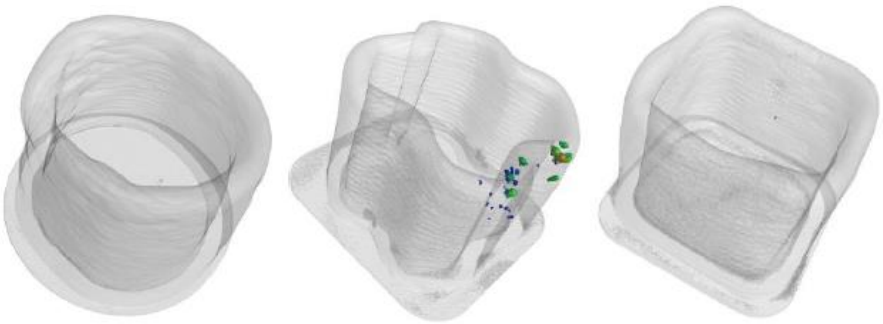

Fig. 11. X-ray images of pores for different geometries: cylinder, cross and rectangle.

The analysis of the occurrence and size of the pores showed that the process was mostly correct and therefore the number and size of pores is not large. For cylindrical surfaces, the easiest for the depositing robot, no pores were found at all. It should be noted, however, that the power of CT lamp required to overexpose the steel caused the resolution to deteriorate, making the detection of very small pores impossible. The largest number of pores was observed for cross shaped surfaces, the most difficult from the point of view of the kinematics of the metal depositing system.

5 Conclusions

The presented measurement results have shown the possibilities of applying measurement techniques using electromagnetic waves to the analysis of structures made with the GMAW method. These structures - as shown by the samples - allow relatively free shape forming, especially if the surfacing head is guided by a robotic arm.

The CT scanner made it possible to reflect the shape of the measured parts and performed the measurement task very well. X-rays moving through the measured object made it possible to find even narrow pockets, naturally occurring after the application of layers in the GMAW technology. It showed also the pores occurring in the structures and in this respect CT is the only non-destructive measuring method. Optical scanners were able to show external structures to varying degrees. The high-resolution scanner reproduced the shape of the objects relatively faithfully. However, it had problems with mapping internal surfaces and in some cases external ones at meso and macro scales, which unfortunately also had some effect on the macro scale. The low resolution scanner, on the other hand, proved to be essentially useless for this application, the dimensions obtained with it were only a very rough estimate of reality. Thin walls made representation of the height of the analyzed elements very difficult, as the measurement device had a problem with detecting the upper part of the walls. This shows how the resolution of the scanner affects the reliability of the reproduced shapes.

Another issue that can be observed is generally rather low repeatability of the welding work blank. In GMAW it is an effect of the difficulty of controlling the arc forming

position. This is why the element is usually machined afterwards in the and a hybrid manufacturing processes is applied.

References

1. Shah, J., Snider, B., Clarke, T., Kozutsky S., Lacki M., Hosseini A., Large-scale 3D printers for additive manufacturing: design considerations and challenges, International Journal of Advanced Manufacturing Technology, 104, 2019, 3679–3693, https://doi.org/10.1007/s00170-019-04074-6
2. Sathies T., Senthil P., Anoop M.S., A review on advancements in applications of fused deposition modelling process, Rapid Prototyping Journal, 26, 4, 2020, 669-687, https://doi.org/10.1108/RPJ-08-2018-0199
3. Prater T., Werkheiser N., Ledbetter F., Timucin D., Wheeler K., Snyder M., 3D Printing in Zero G Technology Demonstration Mission: complete experimental results and summary of related material modeling efforts, International Journal of Advanced Manufacturing Technology, 101, 2019, 391–417, https://doi.org/10.1007/s00170-018-2827-7
4. Rokicki, P., Budzik, G., Kubiak, K., Bernaczek, J., Dziubek, T., Magniszewski, M., Nowotnik, A., Sieniawski, J., Matysiak, H., Cygan, R. and Trojan, A., Rapid prototyping in manufacturing of core models of aircraft engine blades, Aircraft Engineering and Aerospace Technology, 86, 4, 2014, 323-327, https://doi.org/10.1108/AEAT-10-2012-0192
5. Pisula J.M., Budzik G., Przeszłowski Ł., An Analysis of the Surface Geometric Structure and Geometric Accuracy of Cylindrical Gear Teeth Manufactured with the Direct Metal Laser Sintering (DMLS) Method, Strojniški vestnik - Journal of Mechanical Engineering, 65, 2, 78-86, doi:http://dx.doi.org/ 10.5545/sv-jme.2018.5614.
6. Śliwa R.E., Bernaczek J., Budzik G., The application of direct metal laser sintering (DMLS) of titanium alloy powder in fabricating components of aircraft structures, Key Engineering Materials, 2016, 687, pp. 199–205, https://doi.org/10.4028/www.scientific.net/KEM.687.199
7. Santos E.C., Shiomi M., Osakada K., Laoui T., Rapid manufacturing of metal components by laser forming, International Journal of Machine Tools and Manufacture, 46, 2006, 1459–1468.
8. Wanjara P., Brochu M., Jahazi M., Electron beam freeforming of stainless steel using solid wire feed, Materials and Design, 28, 2007, 2278–2286.
9. Ribeiro F., 3D printing with metals, Computing and Control Engineering Journal, 9, 1, 1998, 31-38, DOI: 10.1049/cce:19980108 , Print ISSN 0956-3385, Online ISSN 1741-0460
10. Xia C., Pan Z., Polden J., Li H., Xu Y., Chen S., Zhang Y., A review on wire arc additive manufacturing: Monitoring, control and a framework of automated system, Journal of Manufacturing Systems, 57, 2020, 31-45, https://doi.org/10.1016/j.jmsy.2020.08.008.
11. González J., Rodríguez I., Prado-Cerqueira J-L., Diéguez J.L., Pereira A., Additive manufacturing with GMAW welding and CMT technology, Procedia Manufacturing, 13, 2017, 840-847, https://doi.org/ 10.1016/j.promfg.2017.09.189.
12. Ding J., Colegrove P., Mehnen J., Ganguly S., Sequeira Almeida P.M., Wang F., Williams S., Thermo-mechanical analysis of Wire and Arc Additive Layer Manufacturing process on large multi-layer parts, Computational Materials Science, 50, 12, 2011, 3315-3322, https://doi.org/10.1016/j.commatsci. 2011.06.023.
13. Spencer J.D., Dickens P.M., Wykes C.M., Rapid prototyping of metal parts by three-dimensional welding, Proceedings of the Institution of Mechanical Engineers, Part B: Journal of Engineering Manufacture, 212, 3, 175 - 182, 1998

14. Clark D., Bache M.R., Whittaker M.T., Shaped metal deposition of a nickel alloy for aero engine applications, Journal of Materials Processing Technology, 203, 2008, 439–448
15. Baufeld B., Van der Biest O., Gault R., Additive manufacturing of Ti–6Al–4V components by shaped metal deposition: Microstructure and mechanical properties, Materials and Design, 31, 1, 2010, S106-S111, https://doi.org/10.1016/j.matdes.2009.11.032.
16. Ibrahim I.A., Mohamat S.A., Amir A., Ghalib A., The Effect of Gas Metal Arc Welding (GMAW) Processes on Different Welding Parameters, Procedia Engineering, 41, 2012, 1502-1506, https://doi. org/10.1016/j.proeng.2012.07.342.
17. Cao Y., Zhu S., Liang X., Wang W., Overlapping model of beads and curve fitting of bead section for rapid manufacturing by robotic MAG welding process, Robotics and Computer-Integrated Manufacturing, 27, 2011, 641–645.
18. Leach R., Thompson A., Senin N.: A metrology horror story: the additive surface. Proceedings of ASPEN/ASPE 2017 Spring Topical Meeting on Manufacture and Metrology of Structured and Freeform Surfaces for Functional Applications, 14-17 March 2017, Hong Kong, China.
19. Pagani L., Townsend A., Zeng W., Lou S., Blunt L., Jiang X.Q., Scott P.J., Towards a new definition of areal surface texture parameters on freeform surface: Re-entrant features and functional parameters, Measurement, 141, 2019, 442-459, https://doi.org/10.1016/j.measurement.2019.04.027
20. Guerra M.G., Gregersen S.S., Frisvad J.R., De Chiffre L., Lavecchia F., Galantucci L.M., Measurement of polymers with 3D optical scanners: evaluation of the subsurface scattering effect through five miniature step gauges, Measurement Science and Technology, 31, 1, 2019, https://doi: 10.1088/1361-6501/ab3edb
21. Wieczorowski M., Gapiński B., Grzelka M., Szostak M., Szymański M., The use of photogrammetry in improving quality of workpieces after an injection molding process, Polymers, 63, 2, 2018, 134-144, doi: 10.14314/polimery.2018.2.7
22. Rękas A., Kaczmarek T., Wieczorowski M., Gapiński B., Jakubowicz M., Grochalski K., Kucharski D., Marciniak-Podsadna L., Analysis of Tool Geometry for the Stamping Process of Large-Size Car Body Components Using a 3D Optical Measurement System, Materials 2021, 14, 7608, https://doi.org/10.3390/ma14247608
23. Affatato S., Ruggiero A., Logozzo S., Metal transfer evaluation on ceramic biocomponents: A protocol based on 3D scanners, Measurement, 173, 2021, 108574, https://doi.org/10.1016/j.measurement.2020. 108574.
24. Wieczorowski M., Gapiński B., Swojak N., The use of optical scanner for analysis of surface defects, Annals of DAAAM and Proceedings of the International DAAAM Symposium, 30, 1, 2019, 76-85, doi: 10.2507/30th.daaam.proceedings.010
25. Majchrowski R., Grzelka M., Wieczorowski M., Sadowski Ł., Gapiński B., Large area concrete surface topography measurements using optical 3D scanner, Metrology and Measurement Systems, 22, 4, 2015, 565-576, doi: 10.1515/mms-2015-0046.
26. Yazdanbakhsh S.A., Mohaghegh K., Tiedje N.S., De Chiffre L., Traceability of optical 3D scanner measurements on sand mould in the production of quality castings, Measurement Science and Technology, 32, 8, 2021, https://doi.10.1088/1361-6501/abf707
27. Gapiński B., Wieczorowski M., Marciniak-Podsadna L., Swojak N., Mendak M., Kucharski D., Szelewski M., Krawczyk A., Use of White Light and Laser 3D Scanners for Measurement of Mesoscale Surface Asperities, Lecture Notes in Mechanical Engineering, 2019, 239-256, doi: 10.1007/978-3-030-18682-1_19
28. Herráez J., Martínez J.C., Coll E., Martín M.T., Rodríguez J., 3D modeling by means of videogrammetry and laser scanners for reverse engineering, Measurement, 87, 2016, 216-227, https://doi.org/10.1016/j. measurement.2016.03.005.

29. Lin W., Shen H., Fu J., Wu S., Online quality monitoring in material extrusion additive manufacturing processes based on laser scanning technology, Precision Engineering, 60, 2019, 76-84, doi.org/10. 1016/j.precisioneng.2019.06.004.
30. Swojak N., Wieczorowski M., Jakubowicz M., Assessment of selected metrological properties of laser triangulation sensors, Measurement, 2021, 176, 109190, DOI: https://doi.org/10.1016 /j.measurement.2021.109190.
31. Isa M.A., Lazoglu I., Design and analysis of a 3D laser scanner, Measurement, 111, 2017, 122-133, https://doi.org/10.1016/j.measurement.2017.07.028.
32. Blais F., Beraldin J.A., Recent Developments in 3D Multi-modal Laser Imaging Applied to Cultural Heritage, Machine Vision and Applications 17, 395-409, 2006, https://doi.org/10.1007/s00138-006-0025-3
33. Hongyao S., Jiaao J., Bing L., Zeyu Z., Measurement and evaluation of laser-scanned 3D profiles in wire arc hybrid manufacturing processes, Measurement, 176, 2021, 109089, https://doi.org/10.1016/ j.measurement.2021.109089.
34. Wieczorowski M., Swojak N., Pawlus P., Pereira A., The Use of Drones in Modern Length and Angle Metrology, in: Śniatała P., Iyengar S.S., Bendarma A., Klósak M. (eds.), Modern Technologies Enabling Safe and Secure UAV Operation in Urban Airspace, IOS Press, 125 - 140, doi: 10.3233/NICSP210013.
35. Carmignato S., Dewulf W., Leach R., Industrial X-Ray Computed Tomography, Springer, 2018, ISBN 978-3-319-59571-9, doi.org/10.1007/978-3-319-59573-3.
36. Kruth J.P., Bartscher M., Carmignato S., Schmitt R., De Chiffre L., Weckenmann A.: Computed tomography for dimensional metrology. CIRP Annals – Manufacturing Technology" 60, 2011, s. 821-842, DOI: 10.1016/j.cirp.2011.05.006.
37. Michael G., X-ray computed tomography, Physics Education, 36, 2001, 442-451.
38. Gapiński, B., Wieczorowski, M., Grzelka, M., Alonso, P.A., Tomé, A.B., The application of micro computed tomography to assess quality of parts manufactured by means of rapid prototyping, Polymers, 62, 1, 2017, 53-59, doi: 10.14314/polimery.2017.053
39. Gapiński, B., Wieczorowski, M., Swojak, N., Szymański, M., Geometrical structure analysis of combustible and non-combustible foams by computed tomography, (2018) Journal of Physics: Conference Series, 1065 (14), art. no. 142025, .DOI: 10.1088/1742-6596/1065/14/142025
40. Townsend, A., Pagani, L., Scott, P., Blunt, L., Areal surface texture data extraction from X-ray computed tomography reconstructions of metal additively manufactured parts, Precision Engineering, 2017, 48, 254-264, http://dx.doi.org/10.1016/j.precisioneng.2016.12.008
41. Romano S., Abel A., Gumpinger J., Brandao A.D., Beretta S., Quality control of AlSi10Mg produced by SLM: Metallography versus CT scans for critical defect size assessment, Additive Manufacturing, 28, 2019, 394-405, https://doi.org/10.1016/j.addma.2019.05.017.
42. Hiller J., Maisl M., Reindl L.M., Physical characterization and performance evaluation of an x-ray micro-computed tomography system for dimensional metrology applications, Measurement Science and Technology, 23, 8, 2012, https://doi.10.1088/0957-0233/23/8/085404
43. Gapiński B., Wieczorowski M., Marciniak-Podsadna L., Dybala B., Ziolkowski G., Comparison of Different Methods of Measurement Geometry Using CMM, Optical Scanner and Computed Tomography 3D, Procedia Engineering, 69, 2014, 255–262, DOI: 10.1016/j.proeng.2014.02.230